AL/CF-TR-1996-0087

MODELING OF A DEFORMABLE MANIKIN NECK FOR MULTIBODY DYNAMIC SIMULATION

Hashem Ashrafiuon
Robert Colbert

DEPARTMENT OF MECHANICAL ENGINEERING
VILLANOVA UNIVERSITY
VILLANOVA PA 19085

Louise Obergefell
Ints Kaleps

CREW SYSTEMS DIRECTORATE
BIODYNAMICS AND BIOCOMMUNICATIONS DIVISION
WRIGHT-PATTERSON AFB OH 45433-7901

OCTOBER 1995

FINAL REPORT FOR THE PERIOD MAY 1994 - OCTOBER 1995

AIR FORCE MATERIEL COMMAND
WRIGHT-PATTERSON AIR FORCE BASE, OHIO 45433-6573

DISCLAIMER NOTICE

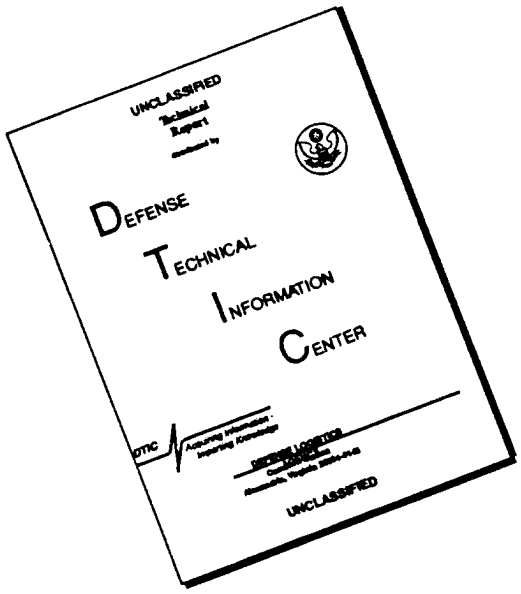

THIS DOCUMENT IS BEST QUALITY AVAILABLE. THE COPY FURNISHED TO DTIC CONTAINED A SIGNIFICANT NUMBER OF PAGES WHICH DO NOT REPRODUCE LEGIBLY.

NOTICES

When US Government drawings, specifications, or other data are used for any purpose other than a definitely related Government procurement operation, the Government thereby incurs no responsibility nor any obligation whatsoever, and the fact that the Government may have formulated, furnished, or in any way supplied the said drawings, specifications, or other data, is not to be regarded by implication or otherwise, as in any manner, licensing the holder or any other person or corporation, or conveying any rights or permission to manufacture, use, or sell any patented invention that may in any way be related thereto.

Please do not request copies of this report from the Armstrong Laboratory. Additional copies may be purchased from:

National Technical Information Service
5285 Port Royal Road
Springfield VA 22161

Federal Government agencies registered with Defense Technical Information Center should direct requests for copies of this report to:

Defense Technical Information Center
Cameron Station
Alexandria VA 22314

TECHNICAL REVIEW AND APPROVAL

AL/CF-TR-1996-0087

This report has been reviewed by the Office of Public Affairs (PA) and is releasable to the National Technical Information Service (NTIS). At NTIS, it will be available to the general public, including foreign nations.

This technical report has been reviewed and is approved for publication.

FOR THE DIRECTOR

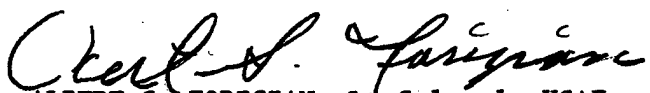

ALBERT S. TORIGIAN, Lt Colonel, USAF
Deputy
Biodynamics and Biocommunications Division

REPORT DOCUMENTATION PAGE

Form Approved
OMB No. 0704-0188

1. AGENCY USE ONLY (Leave blank)	2. REPORT DATE	3. REPORT TYPE AND DATES COVERED
	October 1995	Final - May 1994 - October 1995

4. TITLE AND SUBTITLE
Modeling of a Deformable Manikin Neck for Multibody Dynamic Simulation

5. FUNDING NUMBERS
PE 601102F
PR 2304
TA CB
WU 01

6. AUTHOR(S)
Hashem Ashrafiuon
Robert Colbert
Louise Obergefell
Ints Kaleps

7. PERFORMING ORGANIZATION NAME(S) AND ADDRESS(ES)
Department of Mechanical Engineering
Villanova University
Villanova, PA 19085

8. PERFORMING ORGANIZATION REPORT NUMBER

9. SPONSORING/MONITORING AGENCY NAME(S) AND ADDRESS(ES)
Armstrong Laboratory, Crew Systems Directorate
Biodynmics and Biocommunications Division
Human Systems Center
Air Force Materiel Command
Wright-Patterson AFB OH 45433-7901

10. SPONSORING/MONITORING AGENCY REPORT NUMBER
AL/CF-TR-1996-0087

11. SUPPLEMENTARY NOTES

12a. DISTRIBUTION/AVAILABILITY STATEMENT
Approved for public release; distribution is unlimited

12b. DISTRIBUTION CODE

13. ABSTRACT *(Maximum 200 words)*
The Articulated Total Body (ATB) is a rigid body dynamics computer model of the human body used at the Armstrong Laboratory (AL). The model is used to predict the kinetic response of the human body in different dynamic environments such as aircraft pilot ejections, sled tests, etc. In order to predict the response accurately, however, a rigid body dynamics model may not be sufficient. This is particularly true for the more flexible segments such as the neck and for cases where local segment vibrations occur. In this study, a deformable body dynamics option of the ATB is developed which incorporates linear deformation of individual segments in the ATB model. The displacements due to deformation are determined using finite element modal analysis. The study concentrates on the modeling of manikin necks which have shown large deformation in certain environments. The Hybrid III manikin neck finite element model and modal solution are presented. Modal analysis results are incorporated into the ATB model. Selected parameters for quasi-static Hybrid III neck and several head-neck dynamic simulations are compared with the experimental results where available. It is shown that the new model simulation results have excellent agreement with the experimental results particularly when compared with the rigid model.

14. SUBJECT TERMS
Biodynamics, Mathematical Modeling, Neck

15. NUMBER OF PAGES
29

16. PRICE CODE

17. SECURITY CLASSIFICATION OF REPORT	18. SECURITY CLASSIFICATION OF THIS PAGE	19. SECURITY CLASSIFICATION OF ABSTRACT	20. LIMITATION OF ABSTRACT
UNCLASSIFIED	UNCLASSIFIED	UNCLASSIFIED	UL

THIS PAGE LEFT BLANK INTENTIONALLY

1 Introduction

The Articulated Total Body (ATB) is used at the Armstrong Laboratory (AL) for predicting gross motion of the human body under various dynamic environments. The model treats the individual segments of the human body as rigid bodies. However, the responses predicted by the model may not be accurate since it ignores the effects of small deformations within the individual segments [1-3]. In the case of human body or dummies, the neck undergoes large deformation which may not be modeled accurately through rigid body dynamics. For example, ATB simulation does not provide a good measurement of the Hybrid III Dummy pendulum test [4].

The objective of the paper is introduce the formulation of the new ATB model which can incorporate any number of deformable segments and demonstrate its advantage over the old (rigid) model through simulation and comparison with Hybrid III neck experimental test results.

It is assumed that the deflection of a deformable body relative to its own reference frame is small and linear such that it can be defined by a linear combination of vibration modes. In order to reduce the size and complexity of the problem, a small number of modes may be selected to approximate the displacement field using Ritz approximation [5]. The vibration normal modes are determined using finite element modal analysis of the deformable bodies.

First, the constrained equations of motion of open chain multibody systems representing both rigid body motion and small deformation are developed. Next, finite element modal analysis of the Hybrid III manikin neck is presented. The relevant frequencies and mode shapes obtained from the finite element model of the Hybrid III dummy neck are used in the ATB model simulation. Both static and dynamic loadings are used and the results are compared with the data obtained using the Static Neck Tester [6] and Head/Neck Pendulum [4], respectively.

2 Equations of Motion of Deformable Bodies

To define the gross motion of a deformable segment, a body reference frame, *xyz*, is attached to the undeformed state of the body and its location (x) and orientation (D) is specified with respect to an inertial reference frame *XYZ*. The elastic displacement field of a deformable body (u) may be represented as a linear combination of a set of selected deformation modes determined by finite element modeling and Ritz approximation. Assuming the body is modeled with n nodes and m modes are selected, the displacement field containing nodal translations and rotations of all nodes is written as:

$$u = \Psi a \tag{1}$$

where a is an mx1 modal coordinate vector and Ψ is a $6nxm$ modal matrix. Therefore as shown in figure 1, the position vector of a node k on the body may be written as:

$$x_k = x + D^T s_k = x + D^T(s_{k_0} + \psi_k a) \tag{2}$$

where s_{k_0} and s_k are the position vectors of nodes k in the undeformed and deformed states with respect to *xyz*, D^T is the transpose of the direction cosine matrix, and ψ_k is a size $3xm$ translational modal submatrix corresponding to node k. Taking the first and second time derivatives of Eq. (2), velocity and acceleration vectors of node k are written as:

$$\dot{x}_k = \dot{x} + D^T(-\tilde{s}_k\omega + \psi_k\dot{a}) \tag{3}$$

$$\ddot{x}_k = \ddot{x} + D^T[-\tilde{s}_k\dot{\omega} + \psi_k\ddot{a} + \tilde{\omega}(\tilde{\omega}s_k + 2\psi_k\dot{a})] \tag{4}$$

where ω is the angular velocity vector about *xyz* axes, and "~" operating on a vector produces a skew-symmetric matrix for cross product representation in matrix algebra.

The variational equations of motion of a deformable body at time *t*, for a virtual displacement field that is consistent with the constraints, are written as [7]:

$$-\int_V \rho\, \delta x_k^T \ddot{x}_k\, dV + \int_V \delta x_k^T f_k\, dV = \int_V \delta \varepsilon_k^T \tau_k\, dV \tag{5}$$

where ρ is material density, f_k is the body force at node k, δx_k is virtual displacement of node k consistent with constraints, V is the undeformed volume, and τ_k and ε_k are defined as stress and strain vectors. Taking the variation of Eq. (2), the virtual displacement of node k is written as:

$$\delta x_k = \delta x + D^T(-\tilde{s}_k \delta\pi + \psi_k \delta a) \tag{6}$$

where $\delta\pi$ is a virtual vector along the axis of rotation and its magnitude is the angle of rotation.

For linearly elastic deformation, the modal strain matrix B, relates strain and displacement and the material property matrix D_0 relates the stress and strain vectors as:

$$\tau = D_0 \varepsilon = D_0 B a \tag{7}$$

From Eqs. (4) & (6-7) and the fact that the variational equations must be valid for all admissible δx, $\delta\pi$, and δa, Eq. (5) for a system of interconnected bodies can be written as:

$$\begin{aligned} M_{tt}\ddot{x} + M_{tr}\dot{\omega} + M_{ta}\ddot{a} + B_{11}^T f &= u_t \\ M_{tr}^T\ddot{x} + M_{rr}\dot{\omega} + M_{ra}\ddot{a} + B_{12}^T f + B_{22}^T \tau &= u_r \\ M_{ta}^T\ddot{x} + M_{ra}^T\dot{\omega} + M_{aa}\ddot{a} + B_{1a}^T f + B_{2a}^T \tau &= u_a \end{aligned} \tag{8}$$

and the kinematic constraint equations are:

$$\begin{aligned} B_{11}\ddot{x} + B_{12}\dot{\omega} + B_{1a}\ddot{a} &= \nu_1 \\ B_{22}\dot{\omega} + B_{2a}\ddot{a} + B_{24}\tau &= \nu_2 \end{aligned} \tag{9}$$

Vectors f and τ are reaction forces and moments at the kinematic joints. The mass matrix elements M_{ij} and RHS vectors, u_i, have been derived by Yoo and Haug [8]. Forces due to strain energy and modal damping forces are derived as:

$$\begin{aligned} f_k &= \Psi^T K_s \Psi\, a \\ f_d &= \Psi^T C_s \Psi\, \dot{a} \end{aligned} \tag{10}$$

where K_s and C_s are the finite element stiffness and damping matrices which are diagonalized by modal matrix Ψ in the above equation [9]. The forces in Eq. (10) are simply subtracted from the third equation in Eq. (8). In the above equations, the modal basis is reduced for the deformable segments based on the methods presented in Refs. [10] and [11].

Submatrices B_{ij}'s are defined based on the type of kinematic joints. The first set of constraint equations are defined for free or ball and socket joints as:

$$\begin{aligned} \ddot{x}_i - \ddot{x}_j - D_i^T\tilde{s}_i\dot{\omega}_i + D_j^T\tilde{s}_j\dot{\omega}_j + D_i^T\psi_i\ddot{a}_i - D_j^T\psi_j\ddot{a}_j = \\ - D_i^T\tilde{\omega}_i(\tilde{\omega}_i s_i + 2\psi_i\dot{a}_i) + D_j^T\tilde{\omega}_j(\tilde{\omega}_j s_j + 2\psi_j\dot{a}_j) \end{aligned} \tag{11}$$

The second set of constraint equations are defined for pin joints as:

$$
\begin{aligned}
&(I_3 - hh^T)D_i^T\dot{\omega}_i - (I_3 - hh^T)D_j^T\dot{\omega}_j - D_i^T\tilde{h}_i\tilde{h}_i D_{n_i}{}^T B_{n_i}\mu_i\ddot{a}_i \\
&\quad + D_j^T\tilde{h}_j\tilde{h}_j D_{n_j}{}^T B_{n_j}\mu_j\ddot{a}_j + \lambda hh^T\tau = \\
&\quad D_i^T\tilde{h}_i(\tilde{\omega}_i\tilde{h}_i(\omega_i + 2\omega_{n_i}) + \tilde{\omega}_{n_i}\tilde{h}_i\omega_{n_i} + \tilde{h}_i C_{n_i}) \\
&\quad - D_j^T\tilde{h}_j(\tilde{\omega}_j\tilde{h}_j(\omega_j + 2\omega_{n_j}) + \tilde{\omega}_{n_j}\tilde{h}_j\omega_{n_j} + \tilde{h}_j C_{n_j})
\end{aligned}
\tag{12}
$$

or for fixed joints as:

$$
\begin{aligned}
&D_i^T\dot{\omega}_i - D_j^T\dot{\omega}_j + D_i^T D_{n_i}{}^T B_{n_i}\mu_i\ddot{a}_i - D_j^T D_{n_j}{}^T B_{n_j}\mu_j\ddot{a}_j = \\
&\quad - D_i^T(\tilde{\omega}_i\omega_{n_i} + C_{n_i}) + D_j^T(\tilde{\omega}_j\omega_{n_j} + C_{n_j})
\end{aligned}
\tag{13}
$$

Matrices in the above equation are described in detail by Ashrafiuon, et al. [12].

The new equations of motion, kinematic constraints, and other required changes have been coded into the ATB model. The only new input required for the new ATB model are the deformable segment definitions; e.g, nodes, frequencies, etc. The new model typically takes 2 to 6 times the CPU time of the old model but is justified because of its significant improvement in accuracy.

3 Hybrid III Manikin Neck

The Hybrid III neck is segmented with three 3.4 inch diameter aluminum plates between Butyl rubber sections to simulate the human vertebral disks, as shown in figure 2. The center rubber sections are 2.7 inches in diameter. They are offset 0.2 inches towards the front of the neck and have slits to provide a different response in flexion than in extension bending. There are also aluminum end plates to facilitate assembly with a manikin. A steel cable runs through a 0.625 inch diameter

hole in the neck. The cable is placed in tension by rotating an adjusting nut on a threaded portion of the cable to limit excessive bending of the neck. The total length of the neck is 5.66 inches.

Since modal analysis is linear, it is not possible to model the slits, the cable, or the nodding blocks which are located at the head/neck attachment joint. To model the slits in the neck would require using a contact surface which implies a "force" as a function of time. Since the classical eigenvalue problem does not have a force vector, this is not possible. The cable and the nodding blocks produce nonlinear effects, which again can not be included in the linear analysis. However, these effects can be approximated by attaching a nonlinear rotational spring at the head/neck joint and using trial and error approach to find its parameters.

The Hybrid III neck is bolted at one end in the experimental tests. There are four bolts at the base and the nodes corresponding to these bolts are constrained in all directions. This model can also be explained in terms of the mode shapes of a cantilever beam. figure 3 shows a view of the Hybrid III finite element mesh; it has 2386 elements and 3427 nodes. The material properties used are Young's modulus, density, and poisson's ratio which are respectively 10,000 kpsi, 0.0981 lb/in^3, and 0.33 for aluminum and 1.2 kpsi, 0.0343 lb/in^3, and 0.49 for Butyl rubber.

The first two modes (36.1 Hz and 36.3 Hz) of the Hybrid III neck are the first bending modes of a cantilever beam. Figure 4 shows the first mode shape. The second mode exhibits some twist, probably due to the asymmetric geometry. The difference between flexion and extension of the physical neck is not apparent in the finite element model; this too has to be adjusted in the ATB simulation. The third mode is the first torsion mode excited at a frequency of 57.2 Hz. The second set of bending modes correspond to the fourth and fifth modes at frequencies of 141.0 Hz and 144.3 Hz. Finally the sixth mode shape is the second torsion mode at 184.3 Hz.

4 Static and Dynamic Test Simulations

In the Static Neck Tester (SNT), the Hybrid III neck behaves similarly to a cantilever beam with a load applied at its free end, as shown in figure 5. The load (F) is linearly increased from 0 to 400 lbs in 2 seconds. This simulation is "slow enough" such that dynamic effects are negligible. See Ref. [6] for detailed description of the experiment. The bending modes obtained from finite element modeling are utilized to represent neck deformation.

Figure 6 shows a comparison of the simulation results using the new ATB model and the SNT test results reported by Spittle, et al. [4] for Hybrid III static neck flexion. It can be seen that the bending stiffness is predicted to be much higher by the simulation for small deformation but slightly lower for large deformation. This is partly because dynamic elastic properties of rubber are used for the model, which are normally higher than the static properties, and also nonlinear (but still elastic) behavior of the rubber is ignored.

An ATB simulation model of the Head/Neck Pendulum (HNP) test is shown in figure 7. The HNP tests are dynamic tests where the head inertia may have a significant effect on the response. There are three segments (pendulum arm, neck, and head) and two fixed joints (j1 & j2) connecting them. Therefore, both neck rotation (ϕ') and head rotation (ϕ) are purely due to neck deformation. The mass and geometric properties for the Hybrid III neck and head reported by Kaleps, et al. [13] are used. A damping ratio of $\zeta = 0.9$ is used for the neck which has an effective value of about 0.2 since the head introduces significant increase in system inertia. See Ref. [4] for a detailed description of the experiment.

The excitation is provided through deceleration data obtained from the HNP tests. The deceleration data and the initial impact velocity are applied along the X-axis of the pendulum arm for

flexion/extension tests and Y-axis for lateral tests. Several flexion tests have been performed by dropping the pendulum arm from 20°, 40°, 60°, 80°, and 120° angles and one lateral test by dropping from 65^0 resulting in impact velocities ranging from 54.74 to 275.4 in/sec. The first four bending modes which represent two flexion/extension and two lateral deformation modes are selected. These modes are sufficient for accurate modeling of neck deformation due to physical characteristics of the system and range of frequencies obtained from the deceleration data.

The results obtained by the deformable model were compared with the rigid body model [6] and the HNP test results. The deformable model proved to be much more accurate than the rigid model consistently for all tests. This is evident in figures 8 and 9 where head rotation and forward acceleration are plotted as obtained from the HNP 20° test and deformable and rigid models. Note the significant improvement in predicting the frequency of oscillation in addition to the amplitude.

Figures 11-13 show comparison of head and neck rotation (ϕ and ϕ') obtained from the new ATB simulations and HNP 20°, 60°, and 120° tests. It can be seen that the simulation follows the test data closely in most cases. However, for the first two cases (20° and 60°) the test data seems to suggest that the neck is oscillating about a negative mean value. This could be due to a defect (slight permanent deformation) in the neck. Also note that the fundamental natural frequency of the system is about 5 Hz approximately 7 times smaller than neck's first (bending) natural frequency. This, of course, is because of the addition of head mass to the neck which has a similar effect on the system damping as observed by the peak to peak ratio. Finally, the sharp peak observed in the 120° case (figure 12) may be due to the linear deformation assumption.

Figures 9, 14 &15 compare the head C.G. forward (x) accelerations. The simulation results in all cases follow the same pattern as the test data. However, the initial high acceleration peaks are

not accurately predicted by the simulation. These accelerations may be due to activation of the nodding blocks at the head-neck joint and the pre-torqued cable whose effects are nonlinear and not included in the model.

Figure 16 compares the resulting moments of the 60° flexion and 65° lateral simulation tests. This comparison clearly demonstrates that the high peak occurring at about 0.05 seconds into the simulation is due to the interaction of the neck with the nodding blocks since the peak is not observed in the lateral test.

5 Conclusion

Mathematical formulation of a new capability for the ATB model has been presented which allows for modeling and integration of deformable segments into the old rigid body formulation. A finite element model of the Hybrid III manikin neck has been developed. Modal analysis was completed on this model and the first six modes have been extracted for inclusion in the validation of the new ATB model.

The finite element model of the Hybrid III neck has been incorporated into the ATB for quasi-static (Static Neck Tester) and dynamic (Head/Neck Pendulum test) simulations and comparison with experimental data. The model was shown to be stiffer than the actual neck in the static simulations because only dynamic elastic properties were used. Dynamic simulations showed the deformable model to be much more accurate than the rigid model.

Overall the new deformable element modeling methodology works well in the ATB model and can be applied to model other deformable structures such as a seat back or the human neck and spine. The Hybrid III neck and other deformable models will be used in whole body simulations to fully test and validate the new capability.

REFERENCES

1. R.C. Winfrey, Elastic Link Mechanism Dynamics, Journal of Engineering for Industry **93**(1), 268-272 (Feb. 1971).

2. W. Sunada and S. Dubowsky, The Application of Finite Element Methods to the Dynamic Analysis of Flexible Spatial and Co-Planar Linkage Systems, Journal of Mechanical Design **103**, 643-651 (July 1981).

3. Y.A. Khulief and A.A. Shabana, Dynamic Analysis of Constrained Systems of Rigid and Flexible Bodies with Intermittent Motion, Journal of Mechanisms, Transmissions, and Automation in Design **108**, 38-45 (March 1986).

4. E.K. Spittle and D.J. Baughn, Measurement of Hybrid III Dummy Properties and Analytical Simulation Data Base Development, Report No. AL-TR-1992-0049, National Technical Information Service, Springfield, VA (1992).

5. E.L. Wilson, M.W. Yuan, and J.M. Dickens, Dynamic Analysis by Direct Super-position of Ritz Vectors, Earthquake Engineering and Structural Dynamics **10**, 813-821 (1982).

6. D.J. Baughn, E.K. Spittle, and G. Thompson, A New Technique for Determining Bending Stiffness of Mechanical Necks, SAE Technical Paper No. 930099, SAE International Congress and Exposition, Detroit, MI (1993).

7. I.H. Shames and C.L. Dym, Energy and Finite Element Methods in Structural Mechanics, Hemisphere Publishing Corporation, McGraw-Hill Book Company, NY (1985).

8. W.S. Yoo and E.J. Haug, Dynamics of Flexible Mechanical Systems Using Vibration and Static Correction Modes, Journal of Mechanisms, Transmissions, and Automation in Design **108**, 315-322 (1986).

9. R.W. Clough, Analysis of Structural Vibrations and Dynamic Response, In *Recent Advances in Matrix Methods of Structural Analysis and Design*, (Edited by R.H. Gallagher et al.), pp. 441-465, University of Alabama Press, Huntsville, AL (1971).

10. K.A. Kline, Dynamic Analysis Using a Reduced Basis of Exact Modes and Ritz Vectors, AIAA Journal **24**(12), 2022-2029 (Oct. 1986).

11. H.T. Wu and N.K. Mani, Modeling of Flexible Bodies for Multibody Dynamic Systems Using Ritz Vectors, Journal of Mechanical Design **116**, 437-444 (June 1994).

12. H. Ashrafiuon, R.M. Colbert, L. Obergefell, and I. Kaleps, Modification of the ATB Model to Incorporate Deformable Bodies and Its Verification Through Dummy Neck Modeling and Simulation, Report No. AL-TR-1994, National Technical Information Service, Springfield, VA (1994).

13. I. Kaleps, R. White, R. Beecher, J. Whitestone, and L. Obergefell, Measurement of Hybrid III Dummy Properties and Analytical Simulation Data Base Development, Report No. AAMRL-TR-88-005, National Technical Information Service, Springfield, VA (1988).

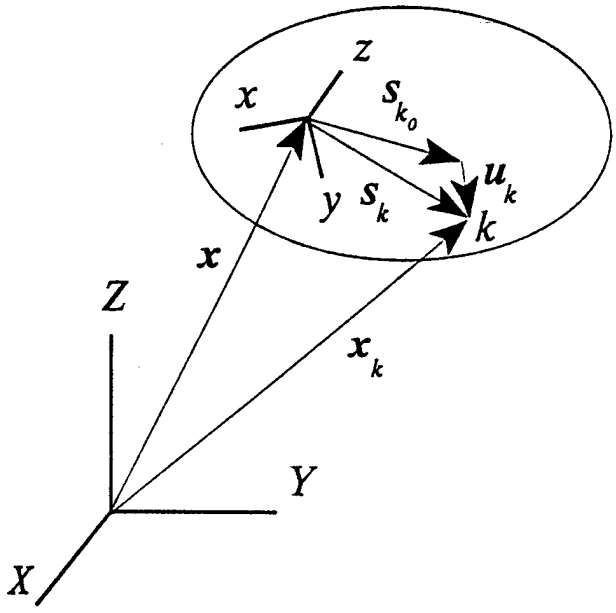

Figure 1. Kinematics of a deformable body

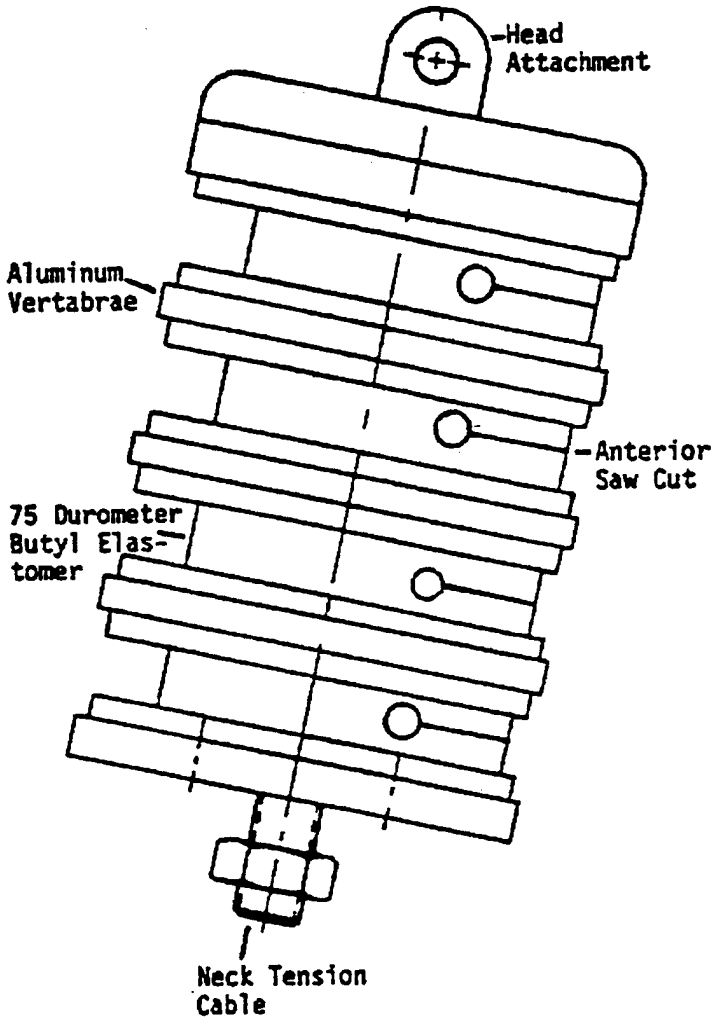

Figure 2. Hybrid III manikin neck

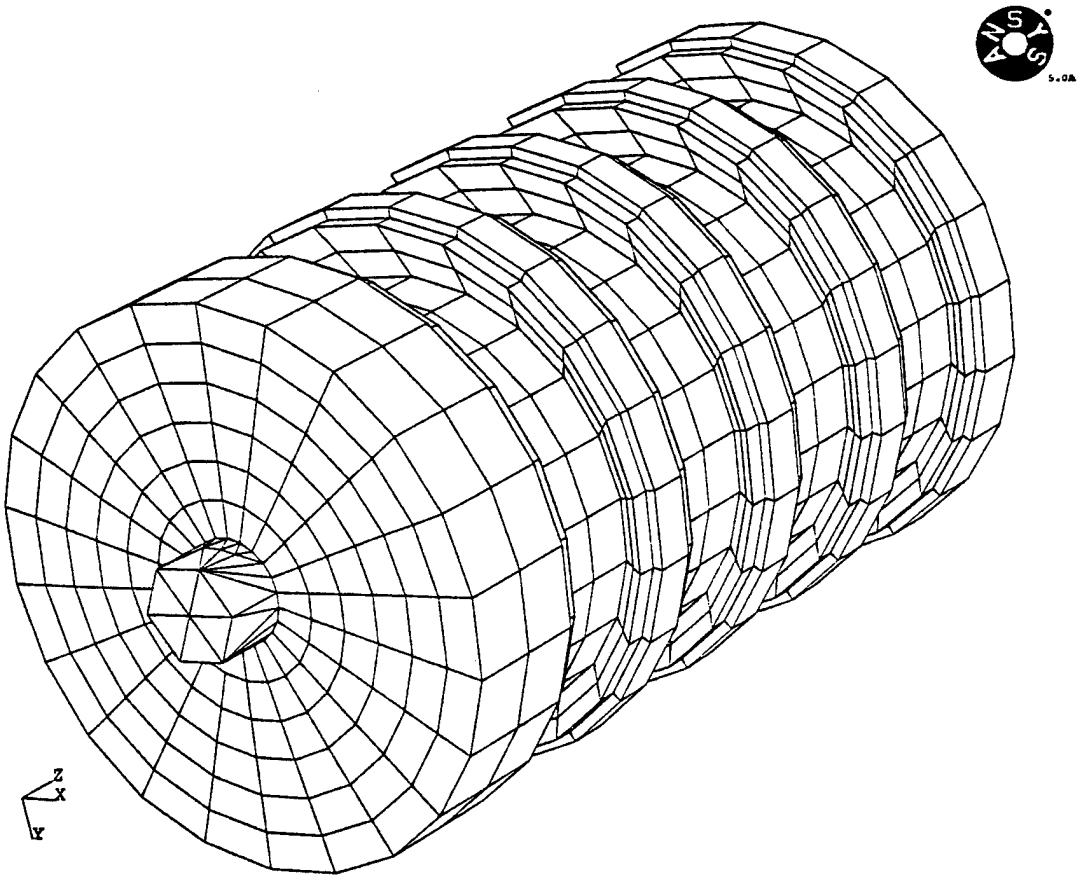

Figure 3. Hybrid III finite element mesh

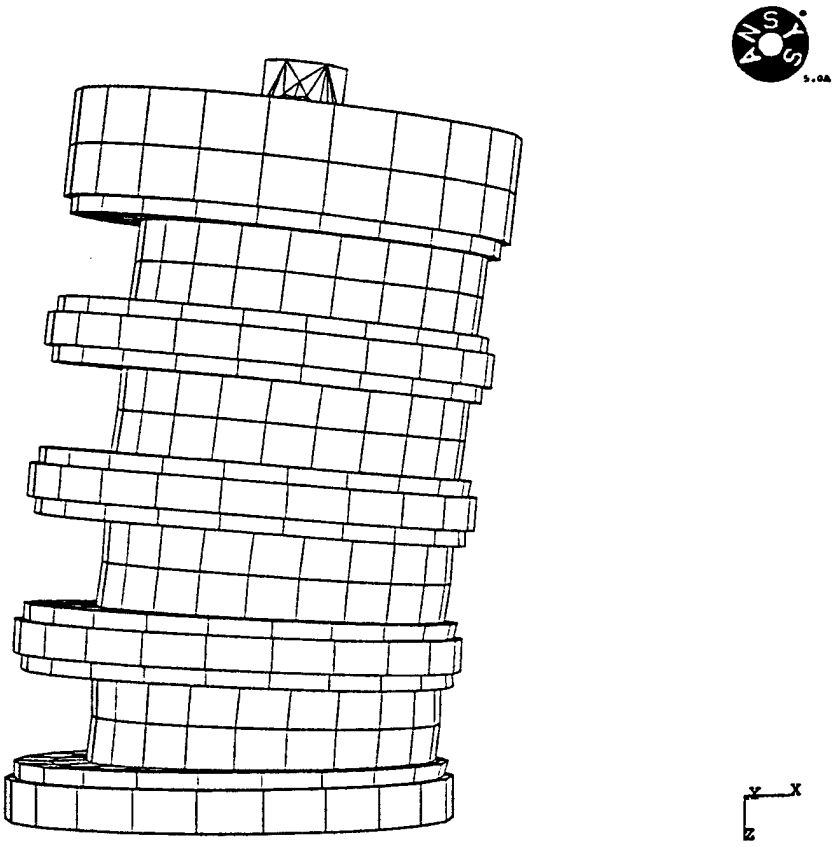

Figure 4. Hybrid III first mode shape (36.1 Hz)

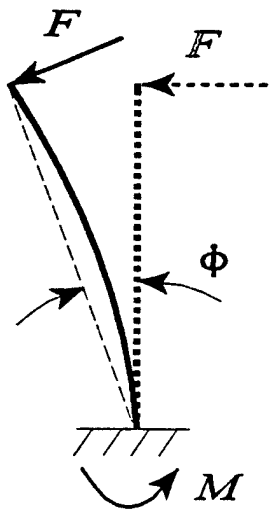

Figure 5. Static test neck model

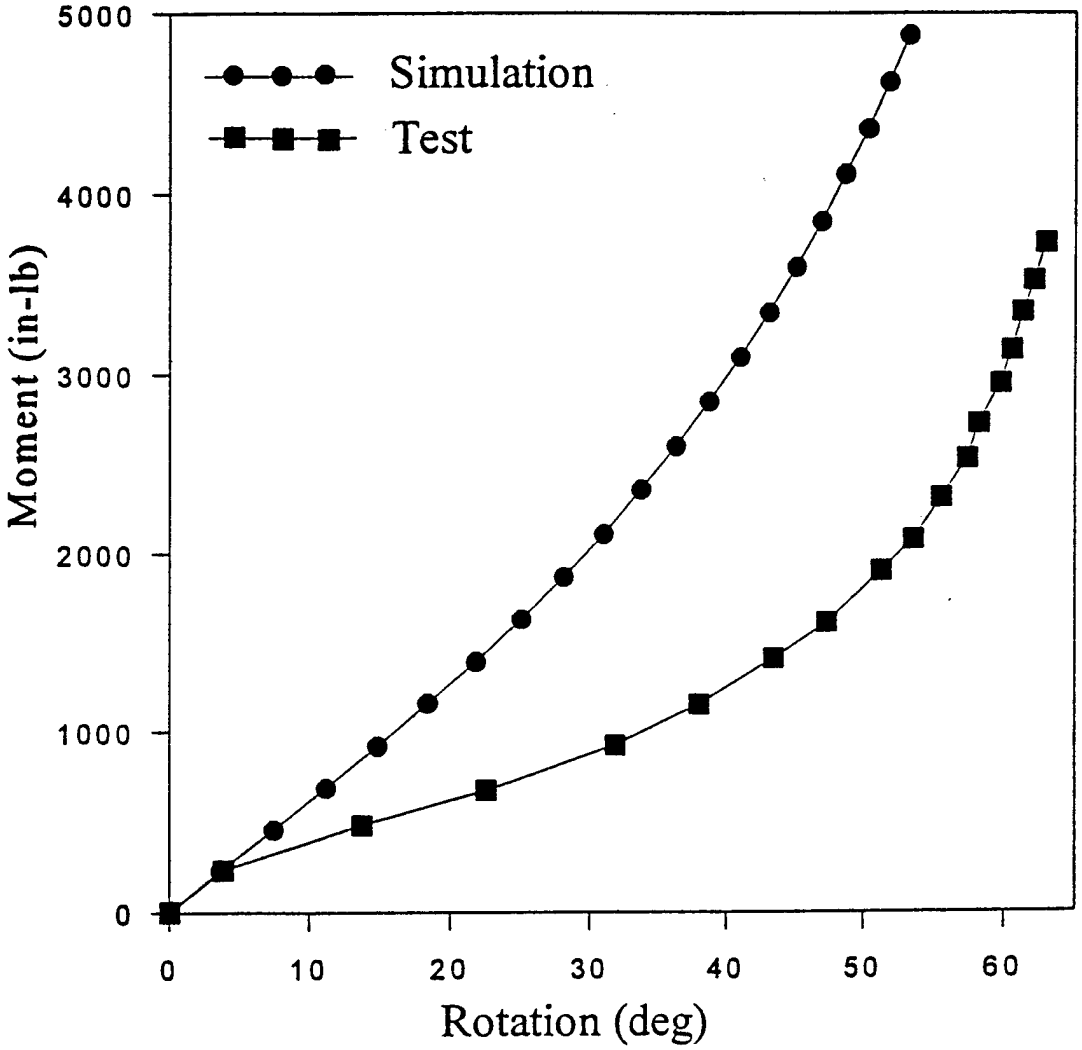

Figure 6. Moment vs. rotation in Hybrid III static test [4] and simulation

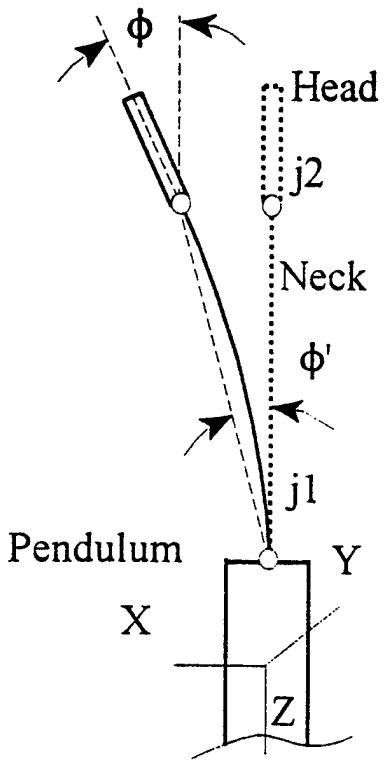

Figure 7. Head/Neck Pendulum test model

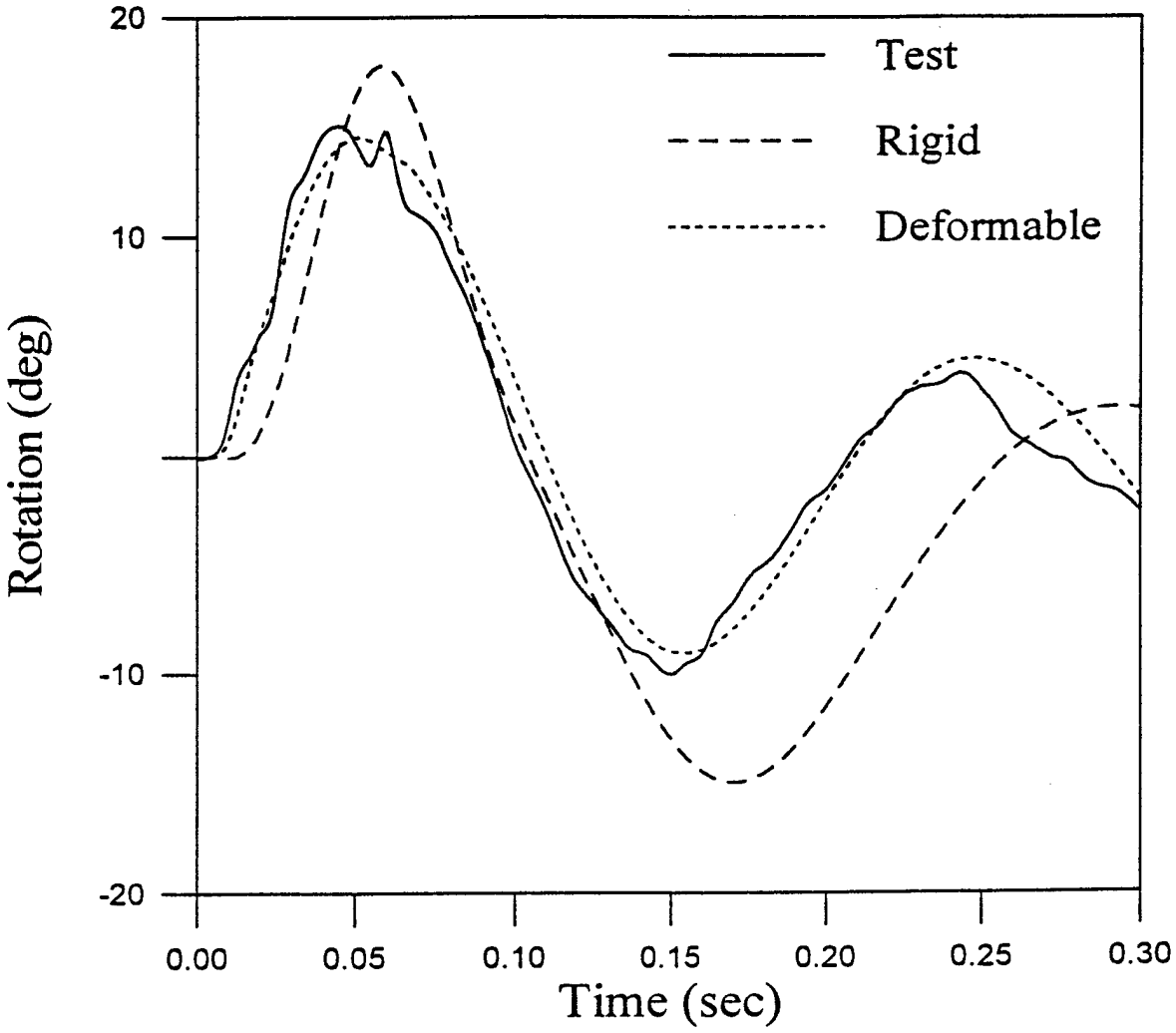

Figure 8. Comparison of Hybrid III head rotations in HNP 20° flexion test

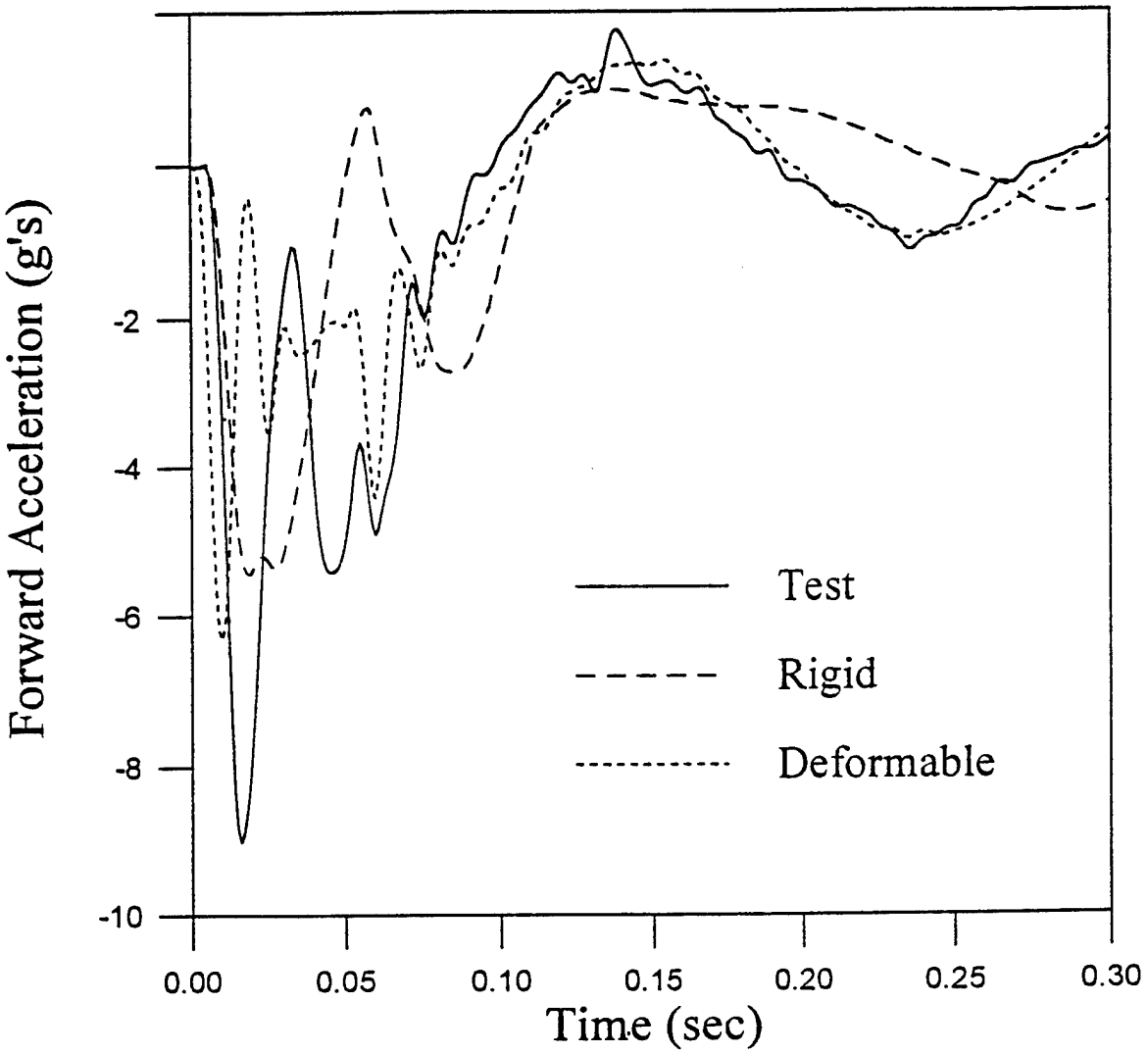

Figure 9. Comparison of Hybrid III head rotations in HNP 20° flexion test

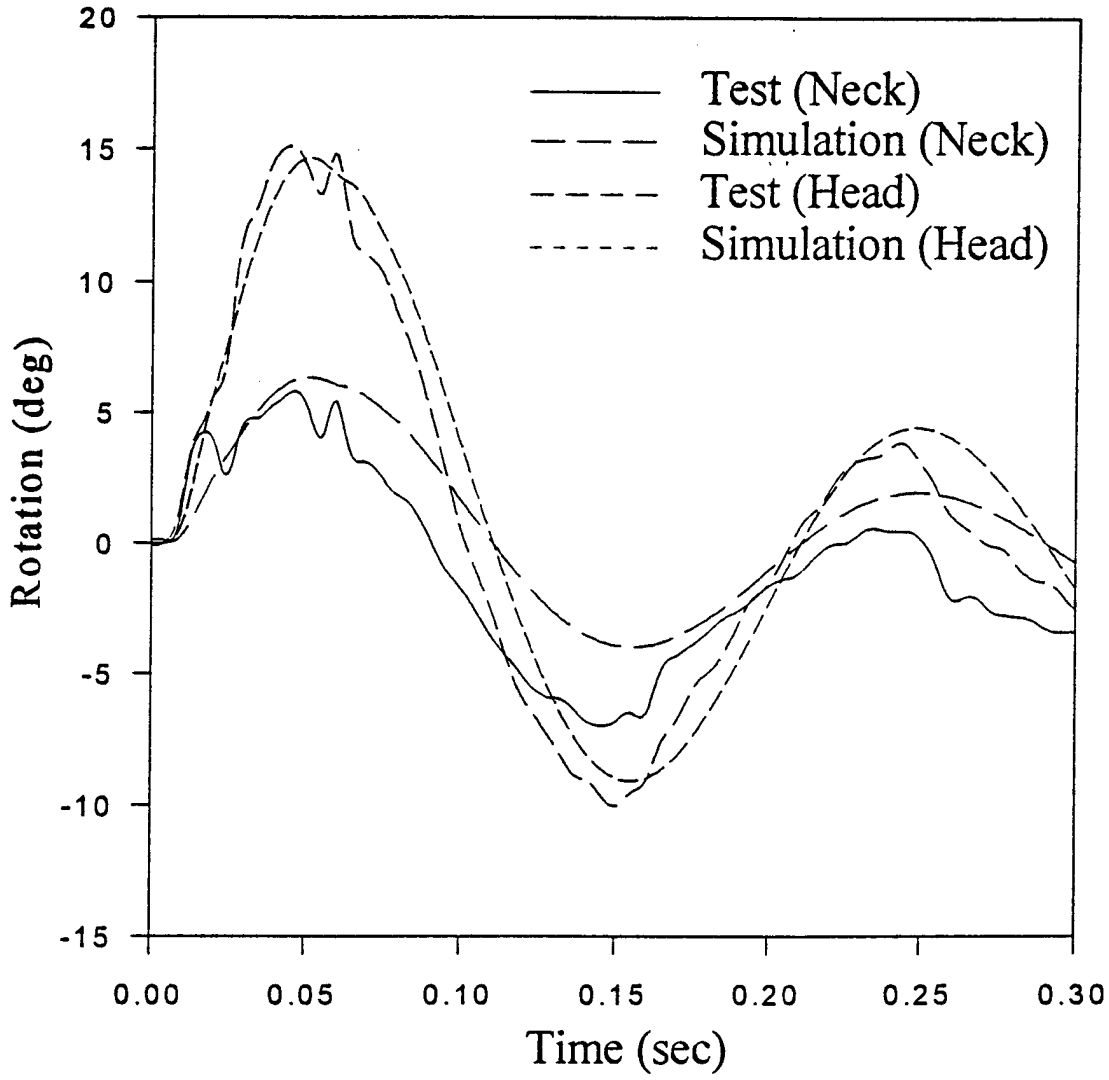

Figure 10. Hybrid III rotations in HNP 20^0 flexion test

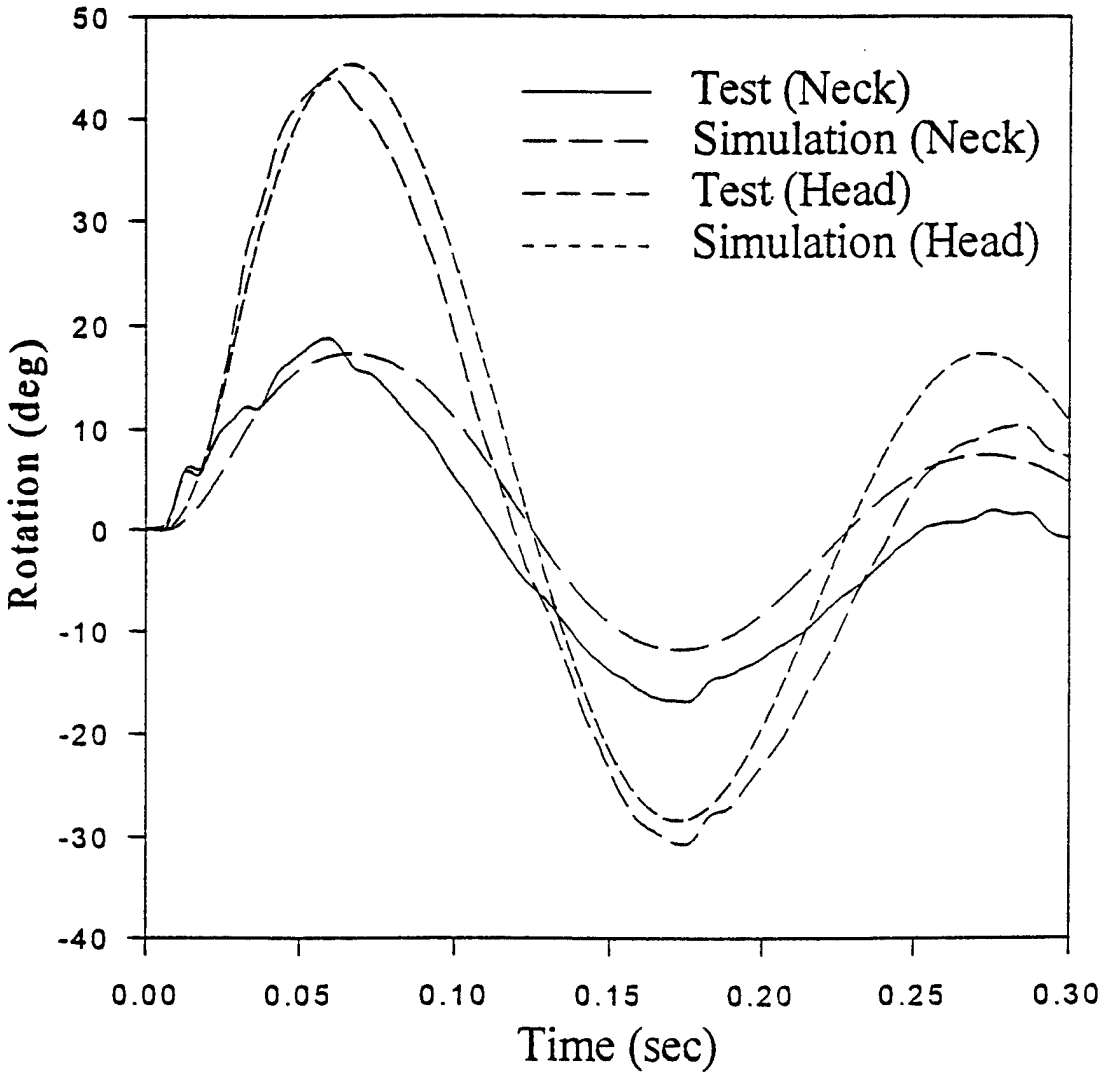

Figure 11. Hybrid III rotations in HNP 60^0 flexion test

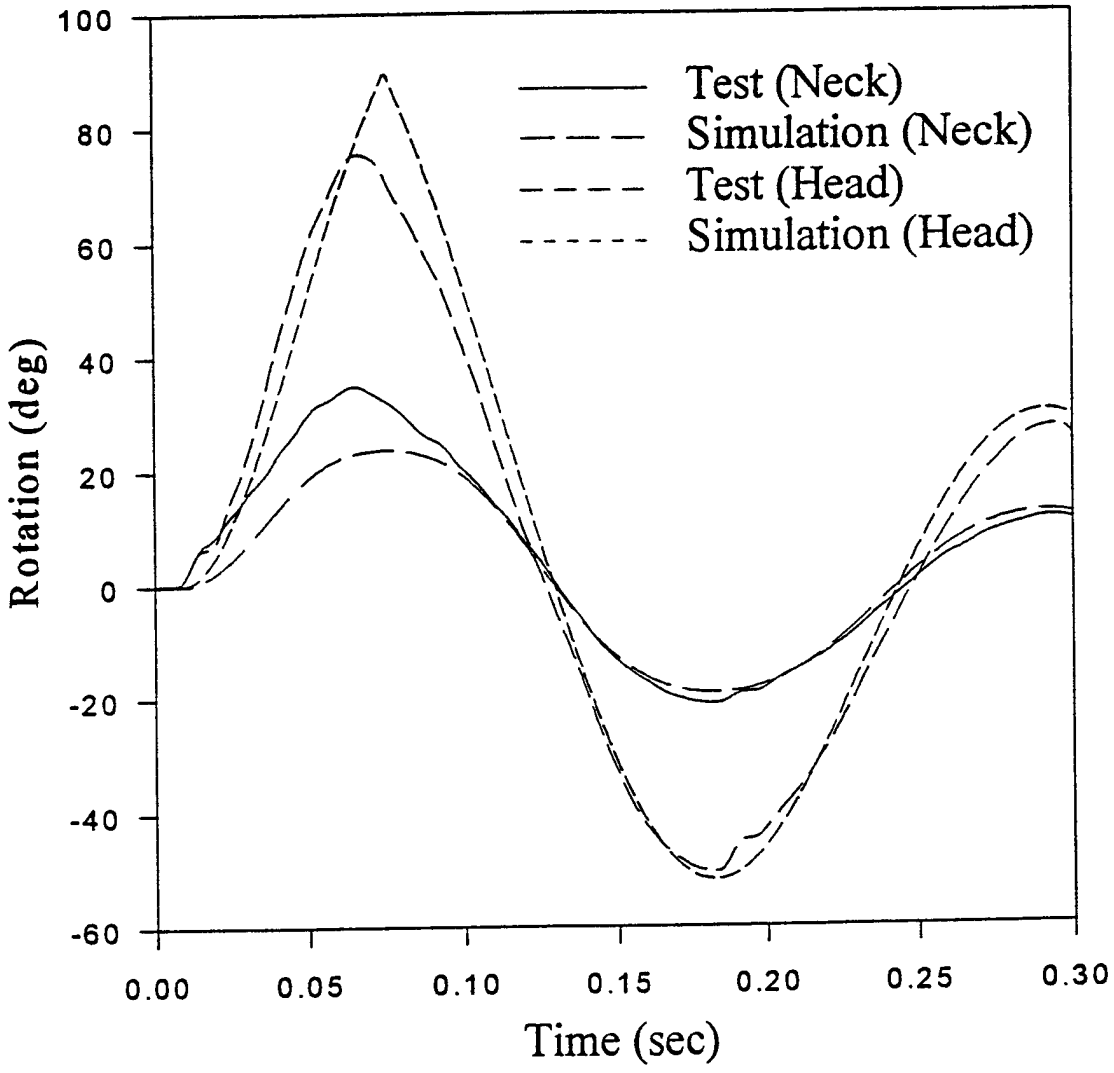

Figure 12. Hybrid III rotations in HNP 120^0 flexion test

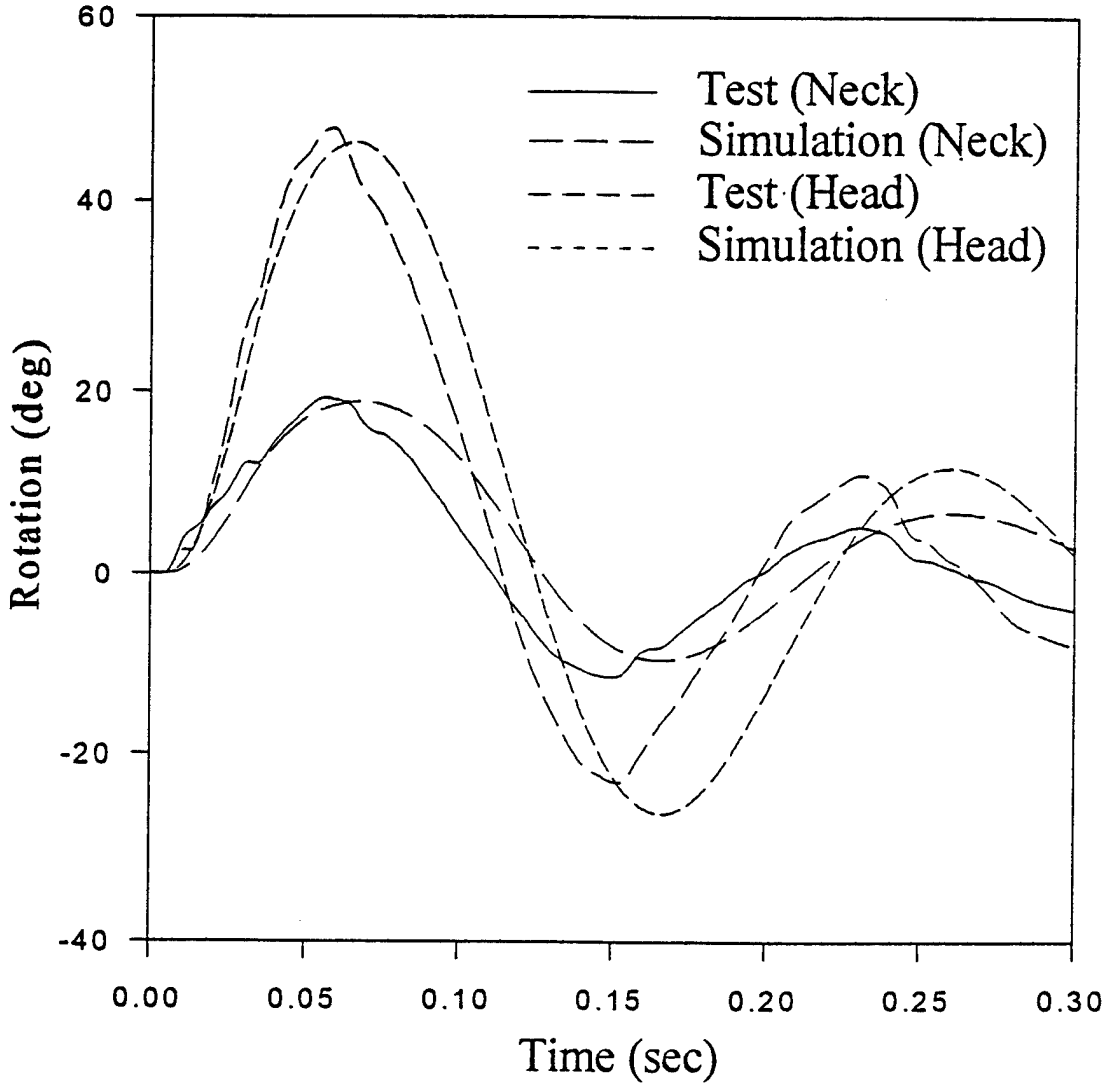

Figure 13. Hybrid III rotations in HNP 65^0 lateral test

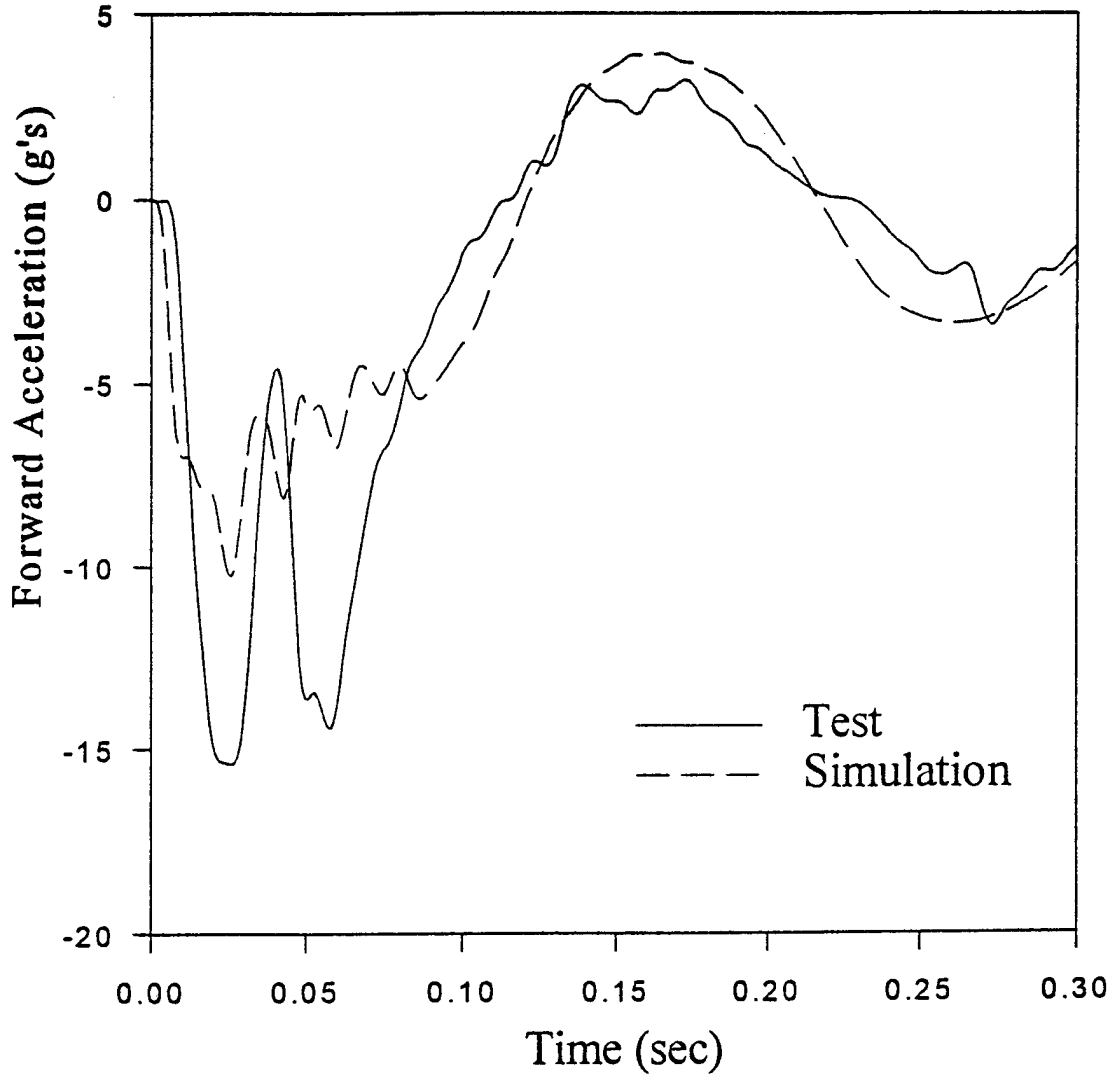

Figure 14. Head *x* acceleration in HNP 60^0 flexion test

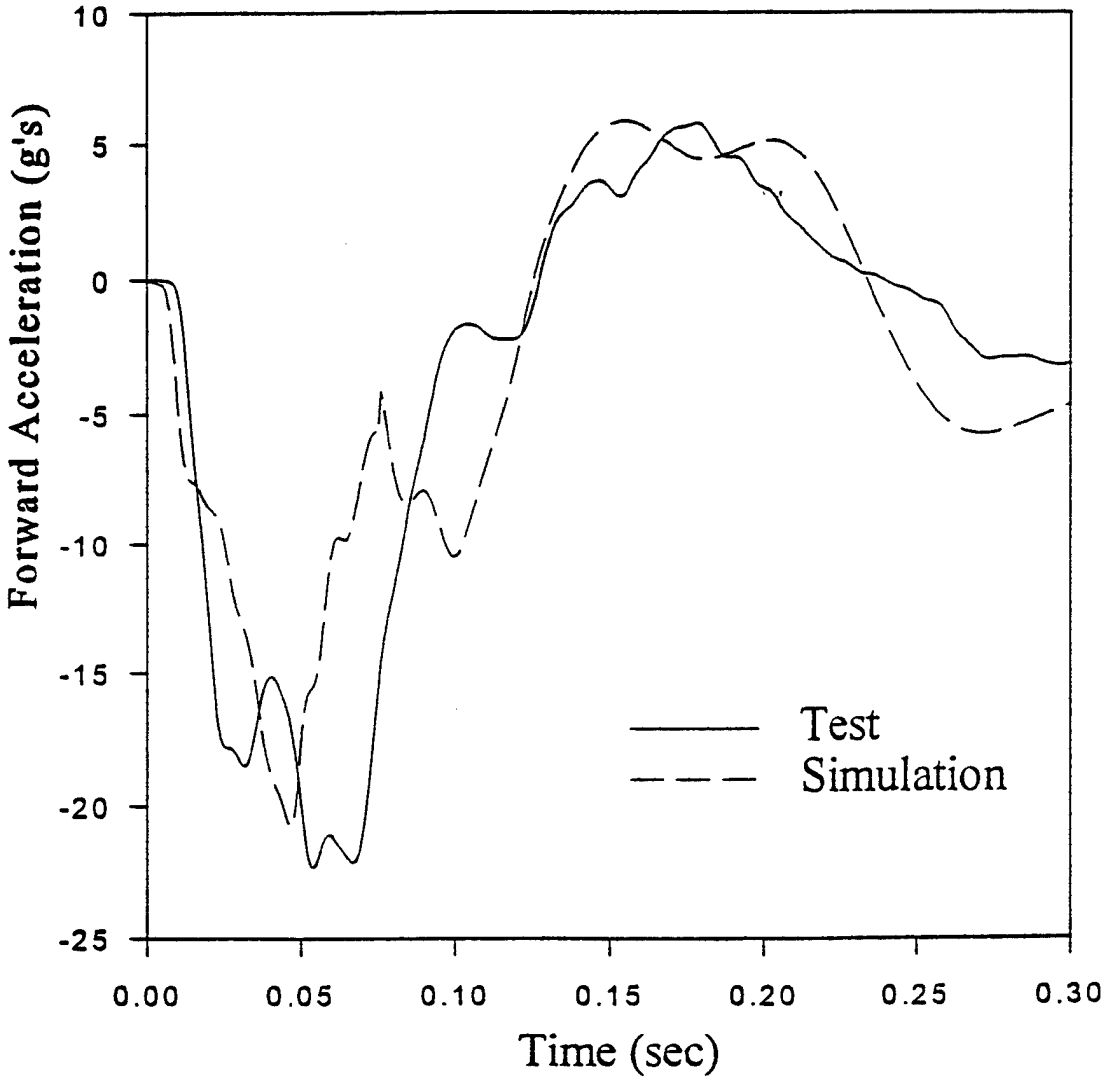

Figure 15. Head x acceleration in HNP 120^0 flexion test

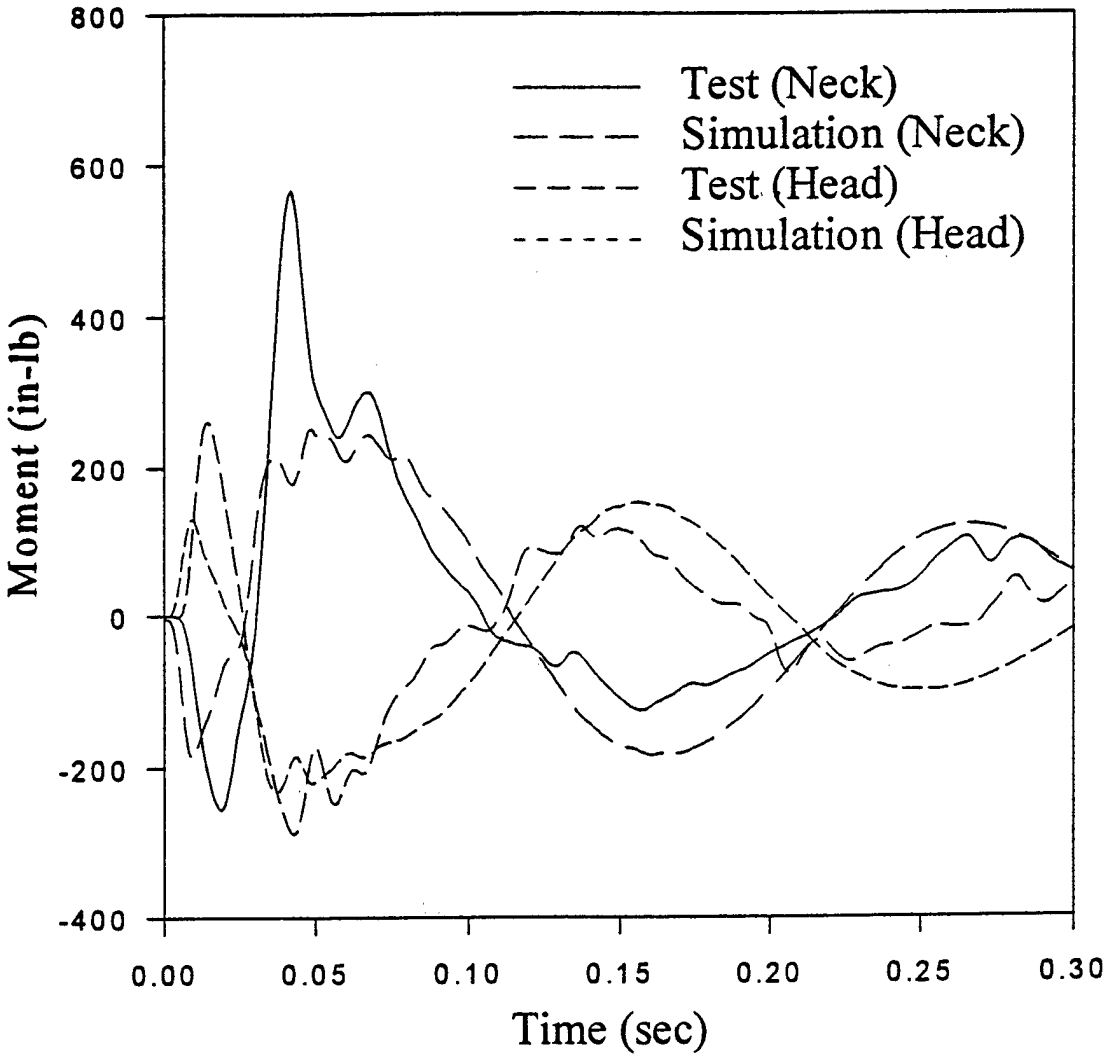

Figure 16. Moments for 60^0 flexion and 65^0 lateral tests

U. S. Government Printing Office 1996 750-071/00210